Stem Cell Reports
Report
ISSCR
OPEN ACCESS

Use of RUNX2 Expression to Identify Osteogenic Progenitor Cells Derived from Human Embryonic Stem Cells

Li Zou,[1] Fahad K. Kidwai,[2] Ross A. Kopher,[1] Jason Motl,[1] Cory A. Kellum,[1] Jennifer J. Westendorf,[3] and Dan S. Kaufman[1,*]
[1]Department of Medicine, University of Minnesota, Minneapolis, MN 55455, USA
[2]Diagnostic/Biological Sciences, School of Dentistry, University of Minnesota, Minneapolis, MN 55455, USA
[3]Department of Orthopedic Surgery, Mayo Clinic, Rochester, MN 55905, USA
*Correspondence: kaufm020@umn.edu
http://dx.doi.org/10.1016/j.stemcr.2015.01.008

SUMMARY

We generated a RUNX2-yellow fluorescent protein (YFP) reporter system to study osteogenic development from human embryonic stem cells (hESCs). Our studies demonstrate the fidelity of YFP expression with expression of *RUNX2* and other osteogenic genes in hESC-derived osteoprogenitor cells, as well as the osteogenic specificity of YFP signal. In vitro studies confirm that the hESC-derived YFP$^+$ cells have similar osteogenic phenotypes to osteoprogenitor cells generated from bone-marrow mesenchymal stem cells. In vivo studies demonstrate the hESC-derived YFP$^+$ cells can repair a calvarial defect in immunodeficient mice. Using the engineered hESCs, we monitored the osteogenic development and explored the roles of osteogenic supplements BMP2 and FGF9 in osteogenic differentiation of these hESCs in vitro. Taken together, this reporter system provides a novel system to monitor the osteogenic differentiation of hESCs and becomes useful to identify soluble agents and cell signaling pathways that mediate early stages of human bone development.

INTRODUCTION

Human embryonic stem cells (hESCs) provide an attractive alternative cell source for bone regeneration. Although recent reports demonstrated methods to generate osteogenic cells from hESCs (Arpornmaeklong et al., 2010, 2011; Mateizel et al., 2008), it is difficult to evaluate the osteogenic development of hESCs and to identify specific cell populations based on surface antigen phenotypes, especially when surface antigens are not cell lineage specific. Also, assessing the homogeneity of cells during differentiation can be challenging. Therefore, a more efficient monitoring system is desirable to evaluate the osteogenic development of hESCs.

RUNX2 is known as a critical regulator (Komori, 2010; Maruyama et al., 2007; Sudhakar et al., 2001) during osteogenic development. *RUNX2* plays an essential role upstream of osteoblastic differentiation in osteogenic specification (Hill et al., 2005), and it induces the expression of osteogenic extracellular matrix genes during osteoblast maturation, such as collagen-Iα, alkaline phosphatase (*ALP*), and osteocalcin (*BGLAP*) (Cohen, 2009; Dalle Carbonare et al., 2012; Lian et al., 2006). Therefore, *RUNX2* initiates osteogenesis in a manner that is precisely controlled temporally and spatially, and loss of *RUNX2* expression at this early stage impairs osteogenic differentiation in bone development (Otto et al., 1997; Cohen, 2013).

To better define the kinetics of osteogenic development from hESCs and to more efficiently identify osteoprogenitor cells for clinical applications, we have generated a novel reporter system for *RUNX2* expression by utilizing the *RUNX2* P1 promoter driven expression of YFP. The P1 promoter directs expression of the longest *RUNX2* isoform and is activated by developmental signaling pathways in mesenchymal progenitor cells (Zhang et al., 2009). We then stably introduced this RUNX2 P1 promoter-YFP cassette with a constitutively active luciferase (*luc*) gene for in vivo imaging into hESCs (H9 cell line). After verifying the reliability of this reporter system, we tracked the osteogenic differentiation using this RUNX2-YFP-integrated H9 hESCs, evaluated the efficiency of such osteogenic differentiation of hESCs, and tested the osteogenic phenotypes of these differentiated cells in vivo.

RESULTS

Integration of the Reporter System Does Not Alter the Differentiation Pattern of hESCs

The RUNX2-YFP reporter was introduced to H9 hESCs using the *Sleeping Beauty* transposon system as previously described (Wilber et al., 2007) (Figures S1A and S1B). Because the engineered hESCs express luciferase (*luc*) from a constitutive EF1α promoter, a highly enriched population of cells expressing the RUNX2-YFP construct was achieved (more than 99% luc$^+$ cells) by bioluminescent imaging and repeated selection of luc$^+$ cells (Figure S1C). To test whether such genetic manipulation altered their differentiation capability, unmodified H9 hESCs and

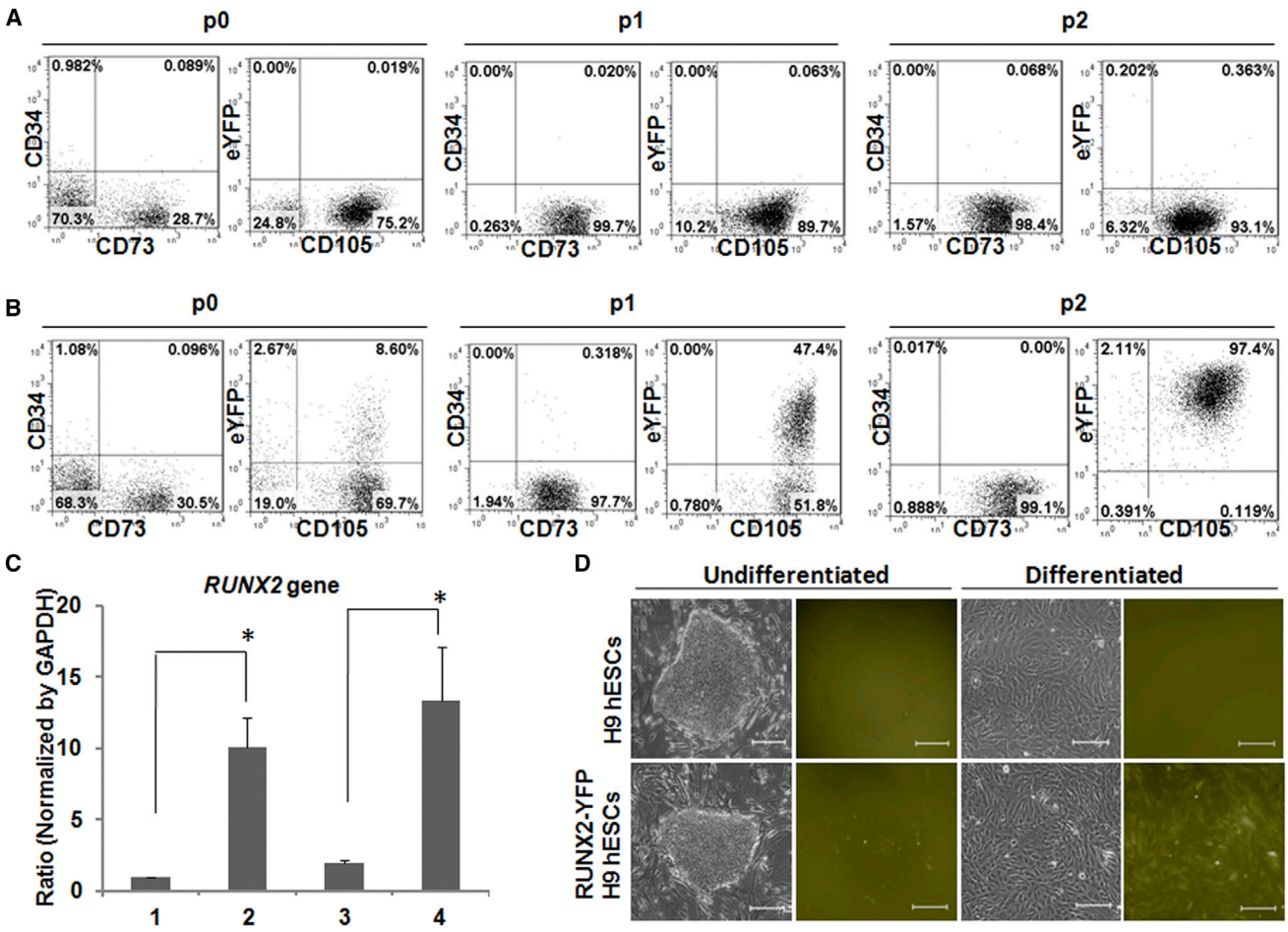

Figure 1. Comparison of the Engineered and Unmodified hESCs

(A and B) Flow cytometric analysis of osteogenic differentiated unmodified hESCs (A) and RUX2-YFP-expressing hESCs (B) at passages 0–2. Representative data from three independent experiments.

(C) qRT-PCR results of *RUNX2* in undifferentiated hESCs (group 1), osteogenic differentiated hESCs at p5 (group 2), undifferentiated RUNX2-YFP hESCs (group 3), and osteogenic differentiated RUNX2-YFP hESCs at p5 (group 4). *GAPDH* gene was used as internal control, and the *Ct* value was normalized to group 1. Data presented as mean ± SEM, n = 3, *$p < 0.05$.

(D) Bright-field and fluorescent images of the unmodified and engineered H9 hESCs, in undifferentiated or differentiated conditions (scale bar, 200 μm).

engineered RUNX2-YFP-H9 hESCs were seeded on gelatin pre-coated culture dishes and cultured in the osteogenic differentiation medium (MSC medium, including 10% characterized FBS, 1% P/S, 1% MEM-NEAA, 2 mM L-glutamine in α-MEM, and osteogenic supplements [OSs] consisting of ascorbic acid, dexamethasone, and β-glycerophosphate, termed MSC+OS medium) followed by serial passaging. Analysis of typical MSC surface antigens and YFP expression in the differentiated hESCs at passage 0, 1, and 2 demonstrated increasing $CD73^+$ and $CD105^+$ cells over time, with comparable cell populations between RUNX2-YFP hESCs and unmodified hESCs. YFP expression was detected only in the engineered cells (Figures 1A and 1B). To verify that this differentiation was generalizable for several clonal populations of the RUNX2-YFP-expressing hESCs, the osteogenic differentiation of four additional RUNX2-YFP-H9 hESC clones have been assessed, all of which demonstrated similar differentiation patterns (Figure S2A). Quantitative RT-PCR (qRT-PCR) analysis of *RUNX2* gene expression in the osteogenic differentiated cells derived from the RUNX2-YFP hESCs and unmodified hESCs showed comparable increase (Figure 1C). Morphologically, both hESC lines did not show any obvious differences, with luciferase positive in the engineered hESCs and YFP fluorescence observed only in the differentiated RUNX2-YFP hESCs (Figures 1D and S1D). Therefore, the similar differentiation capability of both hESC lines allowed for the RUNX2-YFP-expressing hESCs

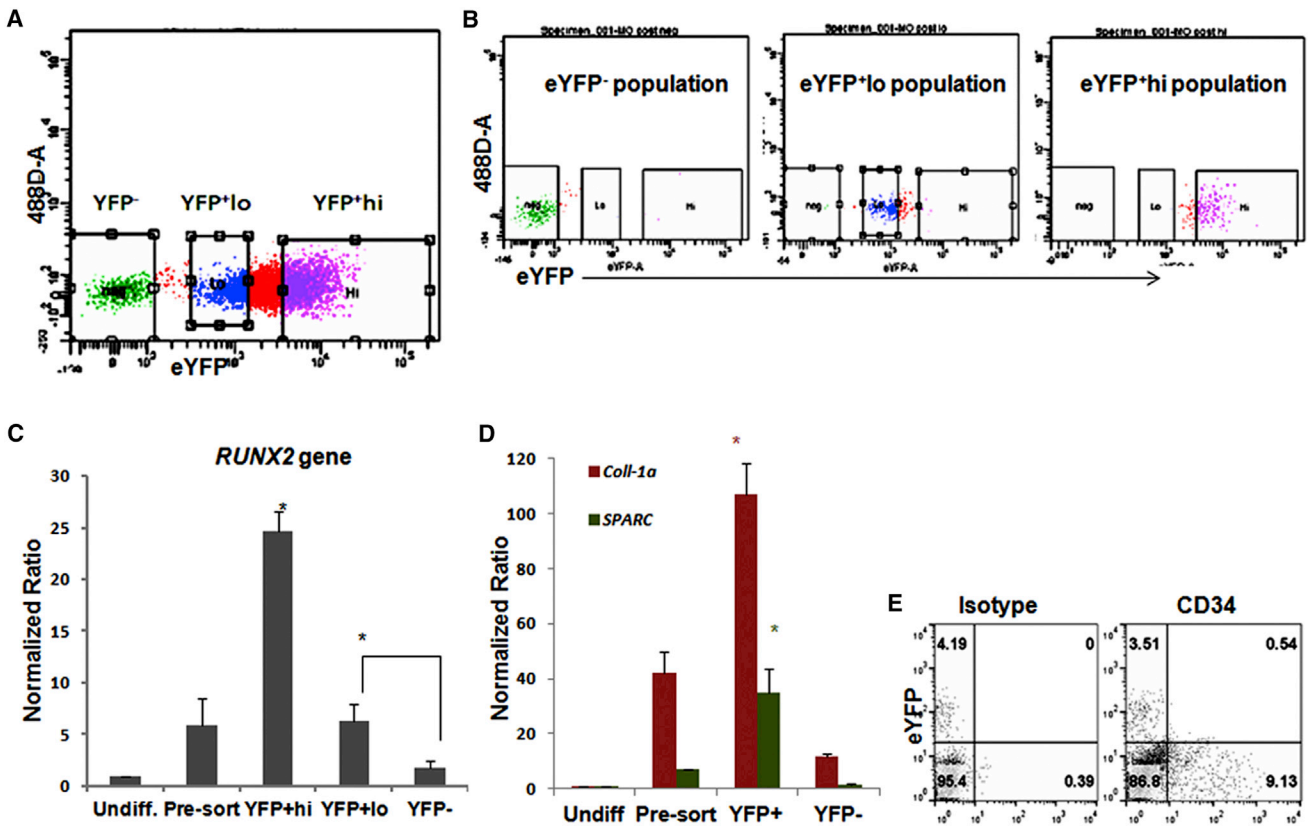

Figure 2. Evaluation of the Reliability of YFP Reporter in Osteogenic Differentiated RUNX2-YFP hESCs

(A) Cell sorting of three cell populations in osteogenic differentiated hESCs at p1, based upon YFP expression intensity.

(B) Post-sort analysis of these three cell populations.

(C) qRT-PCR analysis of *RUNX2* expression in the three cell populations along with undifferentiated cells and pre-sorted cells. *GAPDH* gene was used as internal control, and the data presented here were normalized by the Ct value in undifferentiated group. Data presented as mean ± SEM, n = 3, *p < 0.05.

(D) qRT-PCR results of additional osteogenic genes (*SPARC* and *Collagen-Iα*) in post-sorted YFP^+ and YFP^- with undifferentiated and pre-sorted cells. Data presented as mean ± SEM, n = 3, *p < 0.05.

(E) Flow cytometric analysis of YFP^+ and $CD34^+$ cell populations in hematopoietic differentiated hESCs in co-culture with M210 cells in 15% FBS culture media on day 8.

For (A) and (B), representative results were shown from four biologically independent experiments. (E) is representative of three biologically independent experiments.

to be used in the following studies evaluating their osteogenic differentiation.

YFP Signal Faithfully Reports RUNX2 Activation in the Osteogenic Differentiated Cells

To verify the parallel expression of RUNX2 and YFP, we isolated different cell populations in the osteogenic differentiated hESCs based on the YFP expression intensity and evaluated their *RUNX2* gene expression by qRT-PCR. Flow cytometric analysis confirmed the different YFP expression intensities in the post-sorted cells (Figures 2A and 2B). qRT-PCR results showed that the expression level of *RUNX2* gene corresponded to YFP intensity (Figure 2C). These results demonstrated the fidelity of the YFP reporter to monitor *RUNX2* gene expression in the osteogenic differentiated hESCs. We also evaluated *Collagen-Iα* and *SPARC* genes in the sorted cell populations, which showed similar expression patterns with the highest levels in YFP^+ cell population (Figure 2D). To test the osteogenic specificity, we further evaluated YFP expression in these hESCs cultured in hematopoietic differentiation condition described in our previous study (Tian and Kaufman, 2008). Flow cytometric analysis consistently showed that the hematopoietic differentiated $CD34^+$ hESCs are YFP^- (Figure 2E). Taken together, these assessments demonstrated the reliability of YFP expression to monitor *RUNX2* gene activation in the osteogenic differentiated hESCs.

Differentiated RUNX2-YFP-H9 hESCs Exhibit an Osteogenic Phenotype In Vitro and In Vivo

Although considered a crucial transcription factor in bone development, *RUNX2* is also involved in early chondrogenesis (Villavicencio-Lorini et al., 2010). To test the phenotype of the differentiated cells, we first evaluated chondrogenesis of these YFP$^+$ cells at passage 5 by cell aggregate formation in chondrogenic differentiation medium. However, chondrogenic aggregates were not observed by the YFP$^+$ cells (data not shown). Next, the phenotypes of the osteogenic differentiated hESCs and bone-marrow mesenchymal stem/stromal cell (BM-MSC)-derived osteoprogenitor cells were compared. This analysis demonstrated that both cell populations express typical MSC surface antigens and intracellular osteocalcin at comparable levels, with no CD31, CD34, or CD45 expression (Figures 3A and S3A). As shown in Figure 3B, qRT-PCR analysis demonstrated that the expression levels of osteogenic genes significantly increased in the cells cultured in MSC+OS medium compared to cells cultured in MSC medium alone. The increased levels of *Coll-Iα* and *BGLAP* genes were significantly higher in BM-MSC-derived osteoprogenitor cells than in the hESC-derived cells cultured in MSC+OS medium, whereas a comparable increase of *RUNX2* and *SPARC* genes was found. These qRT-PCR results, which demonstrate elevated osteogenic gene expression in the differentiated hESC cultured in MSC medium, are consistent with other studies (Arpornmaeklong et al., 2010, 2011; Karp et al., 2006). As expected, the pluripotency gene *OCT4* was reduced in both osteogenic-differentiated cell populations (Figure S3B). Functional assays demonstrated the YFP$^+$ cells possess active osteogenic potential comparable to BM-MSC-derived osteoprogenitor cells. In contrast, there is minimal mineral deposition produced by the YFP$^-$ cell population (Figures S3C and S3D).

To better define the kinetics of osteogenic development in this system and to better define the developmental stages of these differentiated cells, qRT-PCR analysis of several early lineage-specific genes, *BRACHYURY* (*T* gene), *HAND2*, *FOXC1*, and *PAX3*, in the osteogenic differentiated hESCs was performed. These studies demonstrated that *BRACHYURY*(*T*) gene expression level only transiently increased, consistent with development of early mesoderm (Ojala et al., 2012; Ramos-Mejia et al., 2010), followed by differentiation of this population. In contrast, expression of *FOXC1* and *PAX3* genes increased over time, suggesting that the early mesodermal differentiation is followed by subsequent differentiation favoring development of paraxial mesoderm (indicated by *FOXC1*) and neural crest (indicated by *PAX3*), with little differentiation into lateral plate mesoderm (as minimal expression of *HAND2* was seen). These cells subsequently form mature osteoblasts after serial passaging, indicated by increased osteocalcin expression (*BGLAP*), in this defined osteogenic culture condition (Figure S2B).

To assess the in vivo osteogenic potential, the differentiated YFP$^+$ hESCs cells were transplanted with gelatin sponge into a critical size calvarial defect in an immunodeficient mouse model. After 3 months, no teratoma formation was identified post-implantation, and the cell survival was demonstrated by the continued presence of luc$^+$ cells in the defect area. μCT results and histomorphometric analysis showed that the bone volume in the defect area repaired by cells in MSC+OS medium was significantly higher than by cells in MSC medium group, with the lowest bone volume in the sponge only group (Figures 3C and 3D). Histological analysis of the healing tissue in MSC+OS group demonstrated laminar bone structures with osteocytes in a well-organized bone matrix and osteoblasts lining the surface of bone tissue. Hematoxylin and eosin (H&E) staining and Masson's Trichrome staining did not show cartilaginous tissue (Figure 3E), which implies intramembraneous bone formation in the calvarial defect area. Morphologically the newly formed bone tissue is different from the adjacent calvarium, which is composed of cancellous bone between cortical bones (Figure 3E). To identify the origin of new bone, we used an osteocalcin (OC) antibody, which recognizes either human or mouse OC in osteoblasts or deposited in the bone matrix as demonstrated in previous studies (Bielby et al., 2004; Hattori et al., 2006; Sackstein et al., 2008). The immunostaining results confirmed the species specificity of the anti-human OC antibody (Figure S4A). The new bone tissue clearly stains positive for human OC (Figure 3F), with an area that stains for both human and mouse OC at the junction between new bone tissues where presumably active osteoblasts from both mouse and human are concentrated (Figures 3F and S4B). This OC distribution pattern is consistent with the histological finding that osteoblasts that produce OC are located in areas of new bone development, whereas osteocytes that produce little OC reside in area of more mature bone. Additional anti-human MHC-I staining also demonstrated similar distribution of human cells in the area of new bone formation (Figure S4C). These results confirm osteogenic potential of these implanted hESC-derived YFP$^+$ osteoprogenitor cells. In addition to engraftment and development of human osteoblasts/osteocytes, it is also likely that the implanted human cells induced proliferation of mouse osteoblasts that contributed to the repair, as seen in similar models (Kuhn et al., 2014). hESC-derived MSCs are known to produce cytokines and growth factors that might induce endogenous bone repair (Kopher et al., 2010; Kimbrel et al., 2014), though specific agents that are active in this model need further elucidation in future studies.

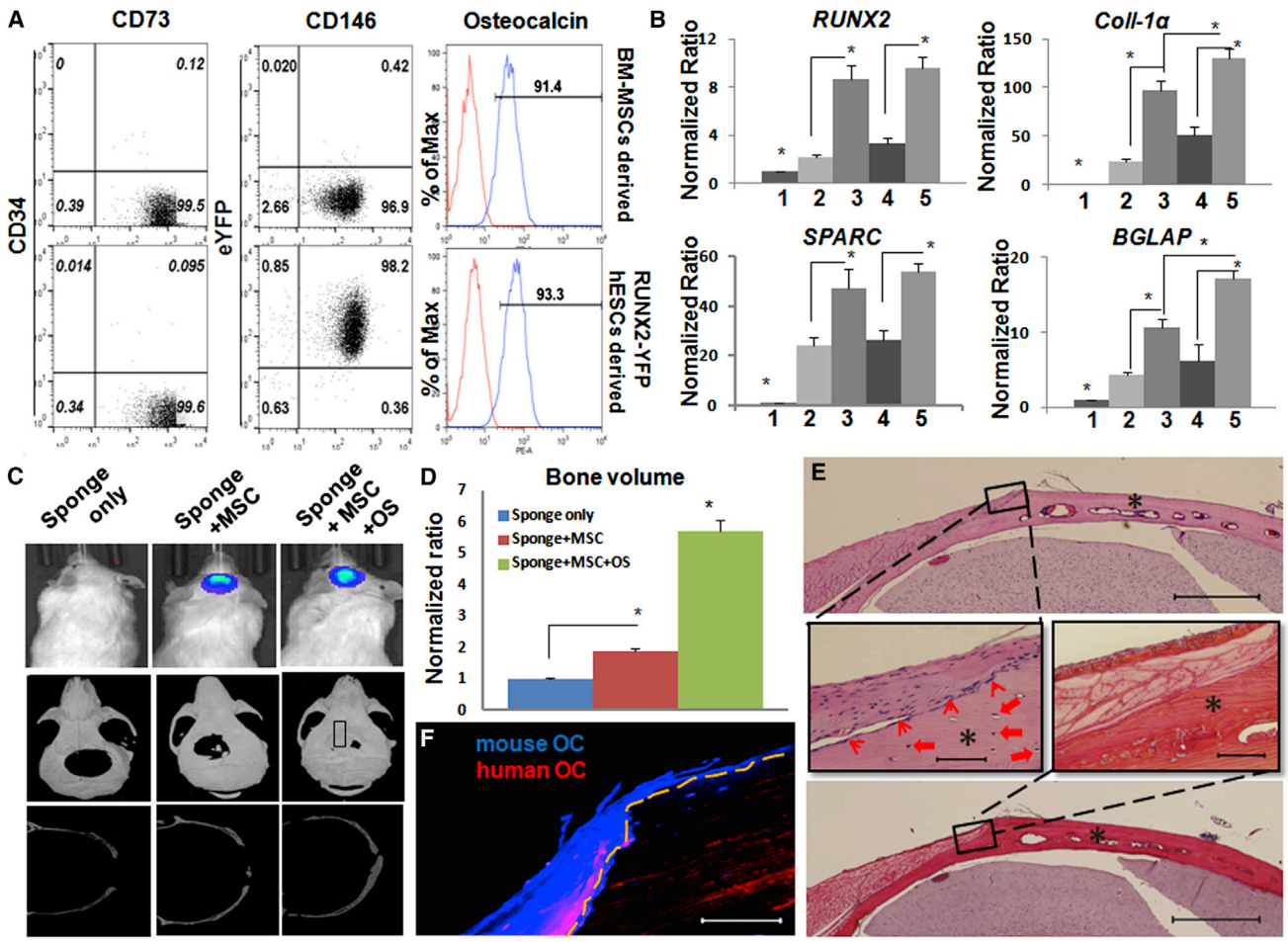

Figure 3. Characterization of Osteoprogenitor Cells Derived from RUNX2-YFP hESCs In Vitro and In Vivo

(A) Flow cytometric analysis of the cell-surface markers and osteocalcin (red, undifferentiated cells; blue, osteogenic differentiated cells) in osteogenic differentiated hESCs at p5 (RUNX2-YFP hESCs derived) and in BM-MSCs cultured in osteogenic medium for 2 weeks (BM-MSCs derived). Representative data are from three independent experiments.

(B) qRT-PCR analysis of the osteogenic gene expression in the undifferentiated hESCs (group 1), the hESCs differentiated in MSC medium (group 2) or MSC+OS medium (group 3), and BM-MSCs in MSC medium (group 4) or MSC+OS medium (group 5). *GAPDH* gene was used as internal control, and data presented here were normalized by Ct value in group 1. Data summarized as mean ± SEM, n = 3, *p < 0.05.

(C) Morphological evaluation of mouse calvarial defect repair. Upper panels are superimposed bright-field and bioluminescent images to demonstrate cell survival and location in the calvarial defect area. Middle panels are 3D reconstructed micro-CT images (the box in group Sponge+MSC+OS indicates where the histology images were acquired). Lower panels are cross-sectional micro-CT images.

(D) Quantitative evaluation of bone volume in the repaired area of calvarial defect by micro-CT. Data presented as mean ± SEM, n = 4 in each group, *p < 0.02.

(E) Histological evaluation of the healing tissue in mouse calvarial defect repaired by cells in group Sponge+MSC+OS. The upper panel is hematoxylin and eosin (H&E) staining, scale bar, 600 μm; the bottom panel is Masson's Trichrome staining, scale bar, 600 μm; the middle panels are higher power views of the H&E staining (left, scale bar, 38 μm) and Trichrome staining (right, scale bar, 38 μm). These higher power images show the junction area of healing tissue. *Area of new bone growth derived primarily from hESC-derived cells; (arrowheads) osteoblasts showing area of new bone development; (arrows) osteocytes in area of more mature mineralized bone.

(F) Immunohistochemical staining of human osteocalcin (red) versus mouse osteocalcin (blue) in the junction area of the repaired mouse calvaria (same region as in middle panels of Figure 3E) (scale bar, 38 μm).

See also Figure S4.

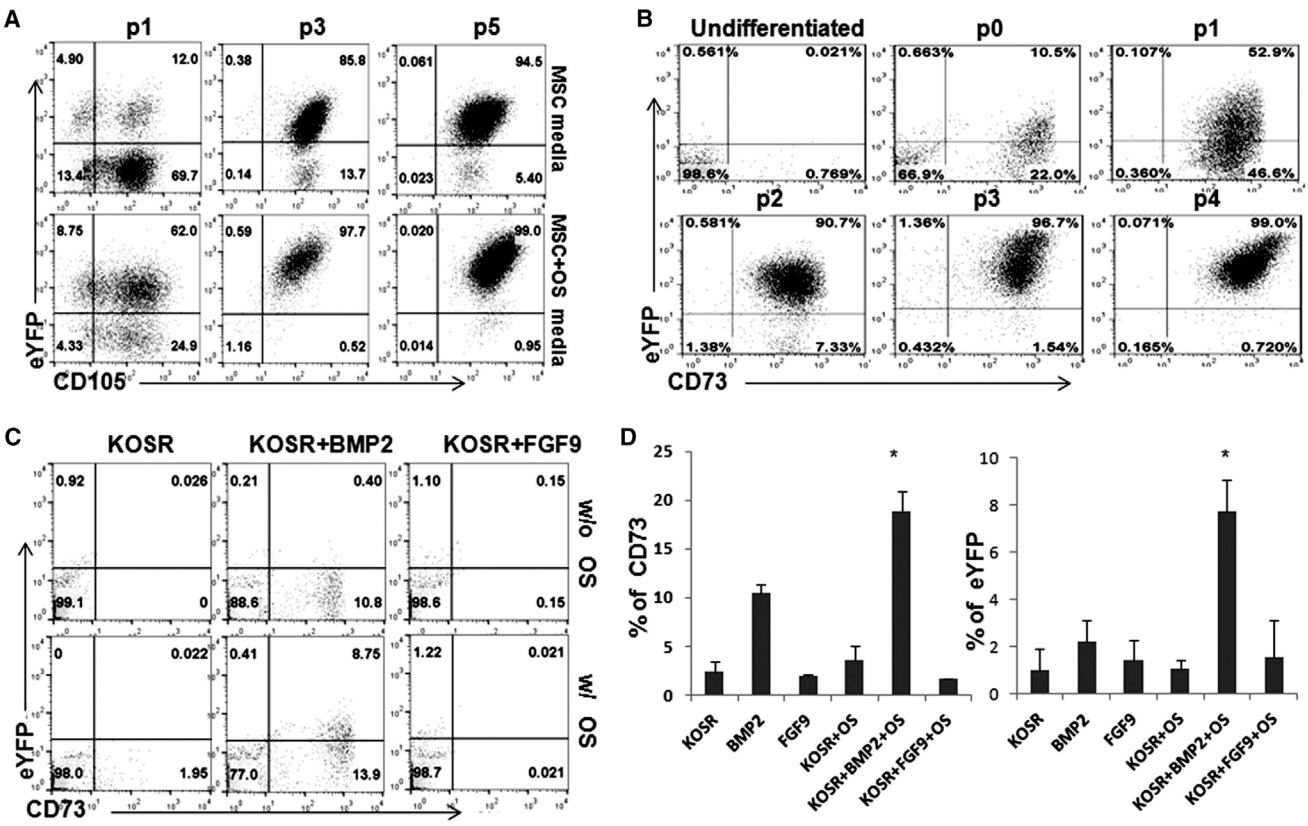

Figure 4. The Role of OS in Osteogenic Differentiation of RUNX2-YFP hESCs

(A) Flow cytometric analysis of cells differentiated in 10%FBS MSC media, with or without OS, at passage 1, 3, and 5. Representative results from two independent experiments.

(B) Flow cytometric analysis of the osteogenic differentiated cells through passage 4. Representative data from three independent experiments.

(C and D) Evaluation of cell differentiation in serum-free condition with or without OS, in the presence or absence of BMP2 or FGF9, at day 10. KOSR, 5% KOSR in place of 10% FBS in MSC media; BMP2, 50 ng/ml; FGF9, 10 ng/ml. Data are presented as mean ± SEM, n = 3, *p < 0.05.

Homogenous Osteoprogenitor Cell Population Derived by OS Treatment of hESC-Derived CD73$^+$ Cells

To test the role of OS in the osteogenic differentiation of hESCs, we compared the differentiation of hESCs in MSC medium with or without OS at different passages. We found that serum (FBS) promoted a CD105$^+$ population as well as YFP$^+$ population in hESCs. Addition of OS markedly increased YFP$^+$ cell population, especially in the early stage (P1), and enhanced YFP expression level in the YFP$^+$ cells (Figure 4A), suggesting that OS in serum-containing medium can significantly boost osteogenic differentiation of hESCs (Figure 4A). These results, combined with the qRT-PCR data (Figure 3B), suggest the superior osteogenic capability may quantitatively and qualitatively contribute to better in vivo bone formation of the cells in the MSC+OS group (Figure 3D).

Flow cytometric analysis of the osteogenic differentiation of hESCs in MSC+OS medium demonstrated a homogenous YFP$^+$ population at passage 4 after serial subculture of hESCs in the osteogenic medium (Figures 4B and S2C). Persistent YFP expression suggests that the differentiated hESCs in osteogenic conditions have committed to an osteogenic lineage. Because essentially all YFP$^+$ cells are CD73$^+$ but not all CD73$^+$ cells are YFP$^+$ in early passages (Figure 4B), these studies suggest that CD73$^+$ cells might serve as the precursors of CD73$^+$YFP$^+$ osteogenic cells.

Next, we tested whether OS may generate YFP$^+$ cells directly without serum-induced differentiation of hESCs and the role of some osteogenic factors in the generation of YFP$^+$ cell population. We cultured RUNX2-YFP hESCs with or without OS in serum-free medium overnight followed by addition of BMP2 or FGF9 for 10 days. Flow cytometric analysis of the differentiated cells showed that cells did not express either CD73 or YFP when cultured in knockout serum replacement (KOSR) or FGF9+KOSR medium, and addition of BMP2 to KOSR induced obvious

increase of $CD73^+$ but not YFP^+ population; addition of OS induced YFP expression only in the BMP2-treated cells, not in the other two groups (Figures 4C and 4D). This short-term analysis in serum-free differentiation media suggests that OS itself could not induce osteogenic differentiation of hESCs unless combined with BMP2, which induces $CD73^+$ cell population. Similarly, BMP2 is not sufficient to induce osteogenic differentiation of hESCs unless combined with OS to mediate development of $CD73^+YFP^-$ cells to $CD73^+YFP^+$ osteogenic progenitor cells.

DISCUSSION

hESCs demonstrate the potential to serve as a starting cell population for bone regeneration, and previous studies report effective differentiation of hESCs to osteogenic lineage (Arpornmaeklong et al., 2010; Kärner et al., 2009). However, it remains important to better define how to obtain homogeneous osteogenic progenitor cells from hESCs. Our studies utilize a novel *RUNX2* (P1)-YFP reporter system to monitor osteogenic differentiation of hESCs. Combined in vitro and in vivo studies validate the fidelity of this system to monitor the osteogenic differentiation and identify the osteogenic cell population derived from hESCs.

Direct differentiation of hESCs has been reported to generate osteogenic cells with comparable osteogenic activity as the cells derived from hBM-MSC or from hESC-derived MSCs (Arpornmaeklong et al., 2011). Here, we simultaneously evaluated expression of *RUNX2* and MSC surface markers to monitor the osteogenic development of hESCs in vitro. The flow cytometry data, gene expression results and in vivo study consistently demonstrated the osteogenic activity in a fraction of hESC-derived cells cultured in serum with no OS. These results are in agreement with previous studies (Arpornmaeklong et al., 2011; Harkness et al., 2011; Kuhn et al., 2014). While addition of OS to serum enhances osteogenic differentiation of hESCs to produce a homogenous osteoprogenitor population, OS itself cannot induce such differentiation prior to development of $CD73^+$ cells from hESCs allowed to differentiate with either serum or BMP2 in vitro. These results suggest that $CD73^+$ cells in the differentiated hESCs might serve as an intermediary cell population to generate osteoprogenitor cells, which provides a plausible mechanism as to why addition of OS at day 14 may dramatically increase bone nodule formation by ESCs in vitro (Bielby et al., 2004; Buttery et al., 2001). Therefore, the term "direct osteogenic differentiation" needs to be cautiously used when hESCs are directly exposed to osteogenic differentiation condition.

The in vitro study of BMP2 provides additional insight and further demonstrates the utility of this *RUNX2*-YFP reporter system. Similar to a short-term study on the effect of BMP2 in human MSCs (Osyczka et al., 2004), we also found that BMP2 does not activate *RUNX2*, indicated by no YFP expression. However, BMP2 does increase $CD73^+$ cell population in hESCs cultured in serum-free conditions. These data suggest BMP2 alone does not induce osteogenic differentiation but may promote the generation of $CD73^+$ cells first and then synergistically facilitates osteogenic differentiation when combined with OS in serum-free condition. Of course, additional detailed long-term studies will be useful to further define the osteogenic factors that mediate osteogenic development.

In conclusion, this *RUNX2*-YFP reporter system is a reliable tool to monitor the osteogenic differentiation of hESCs. It provides a new method to understand the differentiation stages during bone development in a human system. Likewise, this system is useful to isolate early human osteogeneic cells and to further optimize differentiation protocols to better define osteogenic development factors for both hESCs and induced pluripotent stem cells (iPSCs).

EXPERIMENTAL PROCEDURES

Creation of Vector and the Stable Cell Line and Induction of Osteogenic Differentiation of hESCs

hESCs were cultured and induced osteogenic differentiation according to the protocol in Dr. Krebsbach lab (Arpornmaeklong et al., 2011). See Supplemental Experimental Procedures for additional details.

Flow Cytometric Analysis and Fluorescent Imaging

Single-cell suspension of differentiated cells was prepared as previously described (Kopher et al., 2010). See Supplemental Experimental Procedures for additional details.

Real-Time RT-PCR Analysis

Total RNA was abstracted and reverse transcribed into cDNA. Quantitative real-time RT-PCRs were performed. See Supplemental Experimental Procedures for additional details.

Implants Preparation and Surgical Procedure

The differentiated H9-RUNX2-YFP cells at p5∼6 were used for in vivo study. See Supplemental Experimental Procedures for additional details.

Bioluminescent Imaging and microCT Measurement of Defect Repair In Vivo

The bioluminescence images of the implanted cells were visualized, and the bone formation of calvarial defect was assessed using microtomography. See Supplemental Experimental Procedures for additional details.

Histological and Immunohistochemical Study

Histological evaluation of the healing tissue in mouse calvarial defect area was performed according to our previously reported

protocol (Kopher et al., 2010). See Supplemental Experimental Procedures for additional details.

Statistical Analysis

Each experiment was repeated biologically three times independently, if not stated otherwise. As noted in the figure legends, "n" stands for the number of biologically independent experiments. Results were presented as mean ± SEM. Statistic analysis was performed using Microsoft Excel and Prism. One-way or two-way ANOVA was used for multiple comparisons. p values was calculated by two-tailed Student's t test, and the significant difference was defined by $p < 0.05$, as indicated by asterisk.

SUPPLEMENTAL INFORMATION

Supplemental Information includes Supplemental Experimental Procedures, four figures, and one table and can be found with this article online at http://dx.doi.org/10.1016/j.stemcr.2015.01.008.

ACKNOWLEDGMENTS

We graciously thank Dr. Andre J. van Wijnen (Mayo Clinic) for part of the RUNX2 vector, Bonita VanHeel for microCT imaging, Li Li for cell-culture assistance, and Patrick Ferrell and David L. Hermanson for manuscript editing. This work is supported by NIH/NIDCR grants DE022556 (D.S.K.) and R90 DE023058 (F.K.K.).

Received: July 30, 2013
Revised: January 12, 2015
Accepted: January 12, 2015
Published: February 10, 2015

REFERENCES

Arpornmaeklong, P., Wang, Z., Pressler, M.J., Brown, S.E., and Krebsbach, P.H. (2010). Expansion and characterization of human embryonic stem cell-derived osteoblast-like cells. Cell Reprogram. *12*, 377–389.

Arpornmaeklong, P., Pressler, M.J., and Krebsbach, P.H. (2011). Phenotypic and differentiation stability of human embryonic stem cell-derived osteoblasts. Cells Tissues Organs *194*, 326–330.

Bielby, R.C., Boccaccini, A.R., Polak, J.M., and Buttery, L.D. (2004). In vitro differentiation and in vivo mineralization of osteogenic cells derived from human embryonic stem cells. Tissue Eng. *10*, 1518–1525.

Buttery, L.D., Bourne, S., Xynos, J.D., Wood, H., Hughes, F.J., Hughes, S.P., Episkopou, V., and Polak, J.M. (2001). Differentiation of osteoblasts and in vitro bone formation from murine embryonic stem cells. Tissue Eng. *7*, 89–99.

Cohen, M.M., Jr. (2009). Perspectives on RUNX genes: an update. Am. J. Med. Genet. A. *149A*, 2629–2646.

Cohen, M.M., Jr. (2013). Biology of RUNX2 and Cleidocranial Dysplasia. J. Craniofac. Surg. *24*, 130–133.

Dalle Carbonare, L., Innamorati, G., and Valenti, M.T. (2012). Transcription factor Runx2 and its application to bone tissue engineering. Stem Cell Rev. *8*, 891–897.

Harkness, L., Mahmood, A., Ditzel, N., Abdallah, B.M., Nygaard, J.V., and Kassem, M. (2011). Selective isolation and differentiation of a stromal population of human embryonic stem cells with osteogenic potential. Bone *48*, 231–241.

Hattori, H., Masuoka, K., Sato, M., Ishihara, M., Asazuma, T., Takase, B., Kikuchi, M., Nemoto, K., and Ishihara, M. (2006). Bone formation using human adipose tissue-derived stromal cells and a biodegradable scaffold. J. Biomed. Mater. Res. B Appl. Biomater. *76*, 230–239.

Hill, T.P., Später, D., Taketo, M.M., Birchmeier, W., and Hartmann, C. (2005). Canonical Wnt/beta-catenin signaling prevents osteoblasts from differentiating into chondrocytes. Dev. Cell *8*, 727–738.

Kärner, E., Bäckesjö, C.M., Cedervall, J., Sugars, R.V., Ahrlund-Richter, L., and Wendel, M. (2009). Dynamics of gene expression during bone matrix formation in osteogenic cultures derived from human embryonic stem cells in vitro. Biochim. Biophys. Acta *1790*, 110–118.

Karp, J.M., Ferreira, L.S., Khademhosseini, A., Kwon, A.H., Yeh, J., and Langer, R.S. (2006). Cultivation of human embryonic stem cells without the embryoid body step enhances osteogenesis in vitro. Stem Cells *24*, 835–843.

Kimbrel, E.A., Kouris, N.A., Yavanian, G.J., Chu, J., Qin, Y., Chan, A., Singh, R.P., McCurdy, D., Gordon, L., Levinson, R.D., and Lanza, R. (2014). Mesenchymal stem cell population derived from human pluripotent stem cells displays potent immunomodulatory and therapeutic properties. Stem Cells Dev. *23*, 1611–1624.

Komori, T. (2010). Regulation of bone development and extracellular matrix protein genes by RUNX2. Cell Tissue Res. *339*, 189–195.

Kopher, R.A., Penchev, V.R., Islam, M.S., Hill, K.L., Khosla, S., and Kaufman, D.S. (2010). Human embryonic stem cell-derived CD34+ cells function as MSC progenitor cells. Bone *47*, 718–728.

Kuhn, L.T., Liu, Y., Boyd, N.L., Dennis, J.E., Jiang, X., Xin, X., Charles, L.F., Wang, L., Aguila, H.L., Rowe, D.W., et al. (2014). Developmental-like bone regeneration by human embryonic stem cell-derived mesenchymal cells. Tissue Eng. Part A *20*, 365–377.

Lian, J.B., Stein, G.S., Javed, A., van Wijnen, A.J., Stein, J.L., Montecino, M., Hassan, M.Q., Gaur, T., Lengner, C.J., and Young, D.W. (2006). Networks and hubs for the transcriptional control of osteoblastogenesis. Rev. Endocr. Metab. Disord. *7*, 1–16.

Maruyama, Z., Yoshida, C.A., Furuichi, T., Amizuka, N., Ito, M., Fukuyama, R., Miyazaki, T., Kitaura, H., Nakamura, K., Fujita, T., et al. (2007). Runx2 determines bone maturity and turnover rate in postnatal bone development and is involved in bone loss in estrogen deficiency. Dev. Dyn. *236*, 1876–1890.

Mateizel, I., De Becker, A., Van de Velde, H., De Rycke, M., Van Steirteghem, A., Cornelissen, R., Van der Elst, J., Liebaers, I., Van Riet, I., and Sermon, K. (2008). Efficient differentiation of human embryonic stem cells into a homogeneous population of osteoprogenitor-like cells. Reprod. Biomed. Online *16*, 741–753.

Ojala, M., Rajala, K., Pekkanen-Mattila, M., Miettinen, M., Huhtala, H., and Aalto-Setälä, K. (2012). Culture conditions affect

cardiac differentiation potential of human pluripotent stem cells. PLoS ONE *7*, e48659.

Osyczka, A.M., Diefenderfer, D.L., Bhargave, G., and Leboy, P.S. (2004). Different effects of BMP-2 on marrow stromal cells from human and rat bone. Cells Tissues Organs (Print) *176*, 109–119.

Otto, F., Thornell, A.P., Crompton, T., Denzel, A., Gilmour, K.C., Rosewell, I.R., Stamp, G.W., Beddington, R.S., Mundlos, S., Olsen, B.R., et al. (1997). Cbfa1, a candidate gene for cleidocranial dysplasia syndrome, is essential for osteoblast differentiation and bone development. Cell *89*, 765–771.

Ramos-Mejia, V., Melen, G.J., Sanchez, L., Gutierrez-Aranda, I., Ligero, G., Cortes, J.L., Real, P.J., Bueno, C., and Menendez, P. (2010). Nodal/Activin signaling predicts human pluripotent stem cell lines prone to differentiate toward the hematopoietic lineage. Mol. Ther. *18*, 2173–2181.

Sackstein, R., Merzaban, J.S., Cain, D.W., Dagia, N.M., Spencer, J.A., Lin, C.P., and Wohlgemuth, R. (2008). Ex vivo glycan engineering of CD44 programs human multipotent mesenchymal stromal cell trafficking to bone. Nat. Med. *14*, 181–187.

Sudhakar, S., Li, Y., Katz, M.S., and Elango, N. (2001). Translational regulation is a control point in RUNX2/Cbfa1 gene expression. Biochem. Biophys. Res. Commun. *289*, 616–622.

Tian, X., and Kaufman, D.S. (2008). Hematopoietic development of human embryonic stem cells in culture. Methods Mol. Biol. *430*, 119–133.

Villavicencio-Lorini, P., Kuss, P., Friedrich, J., Haupt, J., Farooq, M., Türkmen, S., Duboule, D., Hecht, J., and Mundlos, S. (2010). Homeobox genes d11-d13 and a13 control mouse autopod cortical bone and joint formation. J. Clin. Invest. *120*, 1994–2004.

Wilber, A., Linehan, J.L., Tian, X., Woll, P.S., Morris, J.K., Belur, L.R., McIvor, R.S., and Kaufman, D.S. (2007). Efficient and stable transgene expression in human embryonic stem cells using transposon-mediated gene transfer. Stem Cells *25*, 2919–2927.

Zhang, Y., Hassan, M.Q., Xie, R.L., Hawse, J.R., Spelsberg, T.C., Montecino, M., Stein, J.L., Lian, J.B., van Wijnen, A.J., and Stein, G.S. (2009). Co-stimulation of the bone-related Runx2 P1 promoter in mesenchymal cells by SP1 and ETS transcription factors at polymorphic purine-rich DNA sequences (Y-repeats). J. Biol. Chem. *284*, 3125–3135.